Numerical Simulation of Vortex Shedding Past a Circular Cylinder in a Cross-Flow at Low Reynolds Number With Finite Volume Technique: Part 2 - Flow-Induced Vibrations

Antoine Placzek, Jean-François Sigrist, Aziz Hamdouni

▶ **To cite this version:**

Antoine Placzek, Jean-François Sigrist, Aziz Hamdouni. Numerical Simulation of Vortex Shedding Past a Circular Cylinder in a Cross-Flow at Low Reynolds Number With Finite Volume Technique: Part 2 - Flow-Induced Vibrations. ASME 2007 Pressure Vessels and Piping Conference, Jul 2007, San Antonio, United States. pp.21-30, 10.1115/PVP2007-26021 . hal-04642667

HAL Id: hal-04642667
https://hal.science/hal-04642667v1

Submitted on 15 Feb 2025

HAL is a multi-disciplinary open access archive for the deposit and dissemination of scientific research documents, whether they are published or not. The documents may come from teaching and research institutions in France or abroad, or from public or private research centers.

L'archive ouverte pluridisciplinaire **HAL**, est destinée au dépôt et à la diffusion de documents scientifiques de niveau recherche, publiés ou non, émanant des établissements d'enseignement et de recherche français ou étrangers, des laboratoires publics ou privés.

Distributed under a Creative Commons Attribution - NonCommercial 4.0 International License

Proceedings of ASME
2007 ASME Pressure Vessel & Piping Division Conference
San Antonio, Texas, USA, July 22-26, 2007

PVP2007-26021

NUMERICAL SIMULATION OF VORTEX SHEDDING PAST A CIRCULAR CYLINDER IN A CROSS-FLOW AT LOW REYNOLDS NUMBER WITH FINITE VOLUME TECHNIQUE. PART 2: FLOW-INDUCED VIBRATIONS

Antoine PLACZEK

DCN Propulsion
Service Technique et Scientifique
DCN Propulsion
44620 LA MONTAGNE, France

Laboratoire d'Etude des Phénomènes de Transfert
Appliqués au Bâtiment - Université de La Rochelle
Avenue Michel CREPEAU
17042 LA ROCHELLE Cedex 1, France

Jean-François SIGRIST

Service Technique et Scientifique
DCN Propulsion
44620 LA MONTAGNE, France
jean-francois.sigrist@dcn.fr

Aziz HAMDOUNI

Laboratoire d'Etude des Phénomènes de Transfert
Appliqués au Bâtiment - Université de La Rochelle
Avenue Michel CREPEAU
17042 LA ROCHELLE Cedex 1, France

ABSTRACT

This paper is the sequel of the work exposed in a companion publication dealing with forced oscillations of a circular cylinder in a cross-flow. In the present study, oscillations of the cylinder are now directly induced by the vortex shedding process in the wake and therefore, the former model used for forced oscillations has been modified to take into account the effects of the flow in order to predict the displacement of the cylinder. The time integration of the cylinder motion is performed with an explicit staggered algorithm whose numerical damping is low. In the first part of the paper, the performances of the coupling procedure are evaluated in the case of a cylinder oscillating in a confined configuration for a viscous flow. Amplitude and frequency responses of the cylinder in a cross-flow are then investigated for different reduced velocities U^* ranging from 3 to about 15. The results show a very good agreement at Re=100 and the vortex shedding modes have also been related to the frequency response observed. Finally, some perspectives for further simulations in the turbulent regime (at Re=1000) with structural damping are presented.

1. INTRODUCTION

Vortex-induced-vibrations (VIV) of structures is a phenomenon commonly observed in many fields of engineering: it can cause for example vibrations in heat exchanger tubes, modify the dynamic response of bridge decks or flexible risers used in petroleum production… The case of an elastically mounted cylinder vibrating as a result of fluid forcing is one of the most basic and revealing cases in the general subject of fluid-structure interactions of bluff-bodies. The first part of this study [18] has been conducted with the aim of understanding the phenomena involved when the cylinder is subjected to forced oscillations whose characteristics are known. This previous work has provided interesting results concerning the lock-in behaviour of the cylinder in a certain range of frequency ratios and the different vortex shedding modes appearing in the wake. Similar phenomena are observed when the vibrations are induced by the flow, but in this case, the frequency and amplitude responses are not known a priori.

The vortex shedding process in the wake leads to fluctuating drag and lift forces which cause the oscillations of the cylinder. The phenomenon is self-limited: the fluid flow adjusts so that the oscillation amplitude is restricted to a certain upper limit. It has been observed [14] that the various mechanisms by which the oscillator is able to self-limit its vibration amplitude are a reduction in the amplitude of the aerodynamic forces, appearance of additional frequency components in the time histories of the fluid forces and de-tuning of the vortex-shedding frequency from the structural frequency. Although the phenomenon has been observed for a long time, the maximal amplitude of vibration is not yet clearly defined. Indeed, the cylinder response depends on various parameters and particularly the mass-damping parameter $m^*\zeta$. Figure 1 taken from [9] illustrates the two distinct amplitude responses for high or low $m^*\zeta$. In the first case, only two branches are observed. The behaviour at low

$m^*\zeta$ is more complex and involves three branches. The transitions between the branches are either hysteretic (H) or intermittent (I).

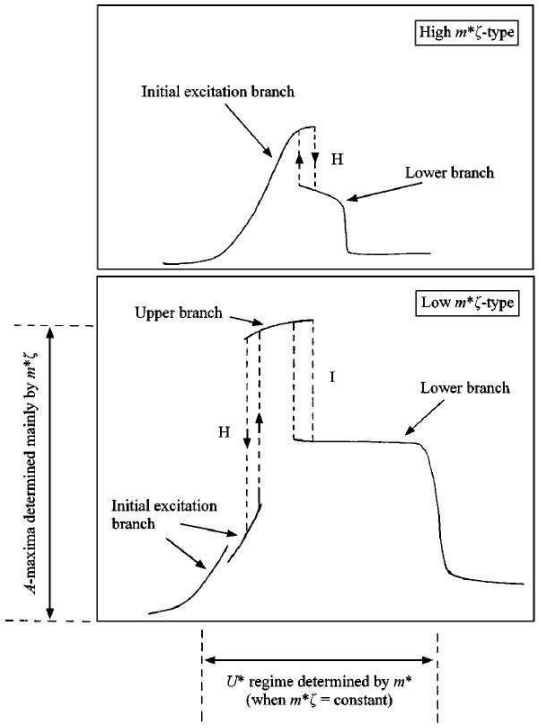

Figure 1. Amplitude responses of the cylinder for high and low $m^*\zeta$ (taken from [9])

For hydrodynamic applications like ours, the values of the mass-damping parameter are generally low and the cylinder response should exhibit three branches. However the parameter $m^*\zeta$ is not only responsible for the number of branches in the amplitude response. There is clearly an influence of the Reynolds number at low Re values and especially in the laminar shedding regime ($\mathrm{Re} \approx 100$). In a companion paper [18], attention has been drawn on the fact that the 2P shedding mode was not observed and the reason seemed to come from the fact that in the presented simulations, the Reynolds number was low. The differences in the vortex shedding mode also exist for VIV and they prohibit the jump to the upper branch. This is confirmed by the 2D Direct Numerical Simulation data from Newman and Karniadakis [15] for $\mathrm{Re}=100$ and 200 and the low Re experiments of Anagnostopoulos and Bearman [3] who did not show the upper branch. The absence of the upper branch in these simulations may be due to the fact that the vortex shedding mode obtained at low Re does not give a net energy transfer from the fluid to body motion over one cycle, unlike the 2P mode at higher Re [9].

The numerical results exposed in the present paper will therefore be compared to those of Shiels et al. [19] who also carried out simulations at $\mathrm{Re}=100$. Moreover the main part of their results is presented in the case of an undamped oscillator like in the present case. The expected response amplitude presented later will be only composed of the lower branch.

To begin with the study, an evaluation of the performances for the coupling procedures between the flow and the cylinder motion is carried out. The various non dimensional parameters commonly used to classify the response regimes of the cylinder are then briefly reminded before turning to numerical results. The first series of simulations is performed for an undamped cylinder at $\mathrm{Re}=100$ and the results are compared to those of Shiels et al. Finally, several results obtained at a higher Reynolds number $\mathrm{Re}=1000$, i.e. in the turbulent regime, are given.

2. DESCRIPTION AND PERFORMANCES OF THE COUPLING PROCEDURES

The numerical simulation of vortex-induced vibrations needs to take into account the effects of the cylinder motion. This could be done artificially by modifying the boundary conditions on the upper and lower side of the computation domain. The mesh remains thus fixed and this avoids the use of the Arbitrary Lagrangian-Eulerian formulation. However, the use of the ALE combined with an explicit procedure for the time integration of the cylinder motion has been preferred here. Before addressing the problem of VIV, the accuracy of the coupling procedures is evaluated, particularly regarding the numerical damping. This artificial damping introduced can have significant effects on the results: indeed it has been mentioned in the introduction that the cylinder response is dramatically different according to the values of the parameter $m^*\zeta$. The problem of the numerical damping introduced by the coupling procedure is not well documented in the VIV literature. However it is a major issue because even if the simulation is supposed to be performed without structural damping, the unwanted numerical damping could lead to a non null value of $m^*\zeta$ and therefore to an unexpected cylinder response.

2.1. Resolution of the Navier-Stokes equations

The Navier-Stokes equations are solved with the same method as in [18]: the simulation uses the incompressible two-dimensional Navier-Stokes equations written in an integral formulation in which the Cartesian velocity components and pressure share the same location at the center of the control volumes. The Navier-Stokes equations are written in the ALE formulation which allows the use of a moving mesh around

the cylinder. The pressure corrections are taking into account thanks to the PISO algorithm. More details on the discretisation scheme and the resolution of the algebraic system can be found in [5] and [21].

2.2. Time integration of the cylinder displacement

The vertical cylinder motion $y(t)$ is governed by the equation of the undamped harmonic oscillator:

$$m\ddot{y}(t) + ky(t) = F_y(t) \qquad \textbf{(1)}$$

where m is the cylinder mass, k is the rigidity of the spring and F_y is the resultant of the lift force. The cylinder natural frequency f_o which will be used later to drive the oscillations of the cylinder is given by:

$$f_0 = \frac{1}{2\pi}\sqrt{\frac{k}{m}} \qquad \textbf{(2)}$$

The resolution of Eq. (1) requires the knowledge of the lift force $F_y(t)$, meaning that the flow field has to be computed before. In fact, this is a typical fluid-structure interaction problem because the lift force influences the cylinder displacement which in turn modifies the flow field and therefore F_y, and so on…

The resolution of such problems can be conducted relatively easily by using staggered procedures, i.e. the fluid and the structure are solved successively for a given time step [4], [17]. This leads inevitably to a time shift between the fluid and the solid, which are not computed exactly at the same time step. The problem can be by-passed with implicit procedures introducing iterations for the same time step and leading to the convergence of the displacement and fluid force (see examples in [1], [7], [10], [22]). Implicit coupling has been particularly used by Sigrist & Abouri [21] who have shown its superiority for non-linear coupled problems. However, for our application, an explicit algorithm adapted from [20] has provided satisfactory results, since it combines a good accuracy and a relatively small CPU time as it will be seen in the following paragraph. Further simulations are currently performed with the implicit procedure to assess its superiority.

The method used for the time integration of Eq. (2) is based on an explicit algorithm, better than the one tested in [21]. Indeed, the numerical damping is dramatically reduced by combining a centered upwind and downwind discretization scheme for the prediction of the displacement. The steps of the algorithm write:

1. Initialization for the first iteration
$$x^n = x_0 \quad v^n = v_0 \quad a^n = a_0 \quad F_y^n = F_0$$
2. Evaluation of the cylinder acceleration
$$a^{n+1} = \frac{F_y^n}{m} - \frac{k}{m}x^n$$
3. Evaluation of the cylinder velocity and displacement
$$v^{n+1} = v^n + \delta t\, a^{n+1}$$
$$x^{n+1} = x^n + \delta t\left[(1-\theta)v^n + \theta v^{n+1}\right]$$
4. Resolution of the flow field with the CFD code to obtain F_y^{n+1}
5. Return to step 2 (next time step)

The procedure is implemented in a user subroutine read by the CFD code at each time step before solving the flow field. Several numerical tests in [20] have shown that $\theta = 0.5$ gives the smallest numerical damping for a perfect flow.

2.3. Results for the cylinder oscillating in a confined configuration

Performances of the previous algorithm with $\theta = 0.5$ (referred to as the *blended procedure* in what follows) are compared with the results given by the implicit algorithm developed by Abouri [1]. The accuracy of the implicit algorithm has been demonstrated by Sigrist & Abouri [21] for a cylinder immersed in an annular space filled with a perfect flow. The case tested is presented on Fig. 2: the cylinder mounted on a spring is shifted from its equilibrium position and is then released.

For equivalent time steps, explicit procedures lead generally to a strong numerical damping. The blended algorithm has been first tested for a perfect flow. The comparison (see Tab. 1) with the undamped analytical solution proposed by Fritz [6] shows that the numerical damping produced by the blended algorithm is about ten times better than the explicit procedure[1] but still about ten times worse than the implicit one. The numerical damping is evaluated thanks to the logarithmic decrement $\delta_{\log}$.

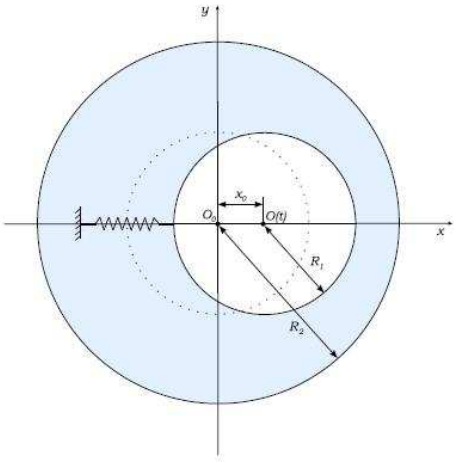

Figure 2. Description of the model used to test the performances of the coupling procedures

[1] The so-called explicit procedure is obtained by doing only one iteration of the implicit algorithm.

Table 1. Comparison of the numerical damping produced by different coupling procedures for a perfect flow

	Implicit	Blended	Explicit
$\delta_{\log}$	2.02E-4	3.81E-3	6.84E-2

The influence of the blending parameter θ is investigated briefly here for $\theta = 0.0$, 0.5 and 1.0. The results presented on Fig. 3 show the same behavior as the one observed in [20]: for $\theta = 0.0$ the damping is negative, whereas for $\theta = 1.0$ it becomes positive. The value $\theta = 0.5$ gives in this case a very good compensation of the positive and negative damping produced by the scheme. However, this value is not universal and has to be adapted to the problem considered.

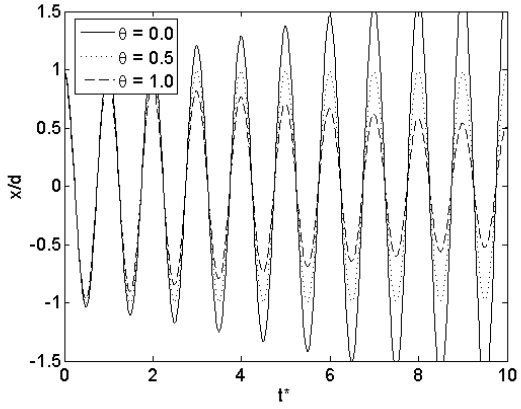

Figure 3. Influence of the blending parameter θ on the numerical damping produced by the blended algorithm

Comparison proceeds with viscous fluids for the same configuration. The mesh is refined near the walls to obtain a good description of the boundary layer. The viscosity of the fluid causes the damping of the oscillations and we need an analytical solution to distinguish the numerical damping from the viscous one. Leblond [11] has developed an analytical expression of the fluid forces acting on a cylinder in the case where the boundary layer δ is small enough relative to the annular space $\Delta R = R_2 - R_1$. The forces exerted on the cylinder wall are evaluated with a convolution product which is numerically computed by an inverse Laplace transform.

Several cinematic viscosities ν are tested in the interval $[10^{-6}, 10^{-5}]$. The pseudo-period, which is influenced by the viscosity, is very well evaluated by the two algorithms (the errors remain inferior to 1%). The damping coefficients calculated from numerical simulations are presented in Tab. 2 for three viscosities. The damping is also evaluated with a linear decrease whose slope is given by *a*. Indeed for viscous flows, the damping is not necessarily governed by an exponential envelope but rather by a combination of linear and exponential decrease.

Table 2. Comparison of the damping computed by the different coupling procedures for a viscous flow

	ν (m^2/s)	1.0×10^{-6}	5.0×10^{-6}	10.0×10^{-6}
$\delta_{\log}$	Analytical	9.69×10^{-3}	21.6×10^{-3}	30.6×10^{-3}
	Blended scheme	17.7×10^{-3}	24.7×10^{-3}	33.8×10^{-3}
	Implicit scheme	7.46×10^{-3}	31.5×10-3	43.9×10^{-3}
a	Analytical	-9.26×10^{-5}	-19.6×10-5	-26.6×10^{-5}
	Blended scheme	-16.3×10^{-5}	-22.0×10-5	-28.9×10^{-5}
	Implicit scheme	-7.15×10^{-5}	-27.1×10-5	-35.7×10^{-5}

The results indicate that the implicit procedure is still better for small viscosities. As ν increases, the blended algorithm seems to provide a better description of the viscous damping. However it should be mentioned that the condition $\delta << \Delta R$ is not respected anymore since the boundary layer represents 30% of the annular space. The analytical model is perhaps not adapted in the last cases, what could explain the discrepancies between the analytical solution and the implicit calculation. On the contrary, the blended procedure is all the more accurate as the viscosity is high. This result is surprising and it could be due to the combination of numerical and viscous damping. Instead of only evaluating the damping with $\delta_{\log}$ and a, a second criterion which shows the evolution of the error is used: the instantaneous absolute error is plotted on Fig. 4 for $\upsilon = 5.0\times10^{-6}$ m^2/s.

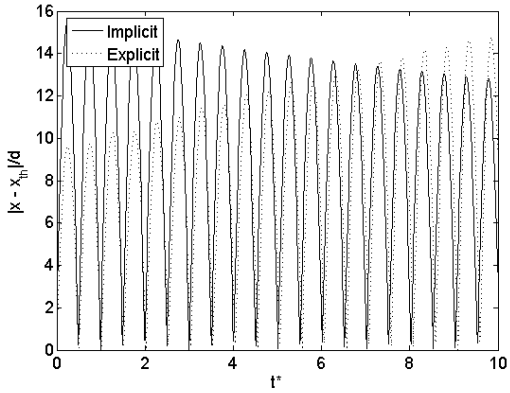

Figure 4. Absolute instantaneous error of the blended and implicit procedures for ν=5x10^{-6}

Although the blended procedure gives in this case a more accurate value for the damping than the implicit algorithm, the error produced by the former becomes progressively higher. On the other hand, the behaviour of the implicit algorithm is very satisfactory because as the simulation goes on, the absolute error decreases. The evolution observed on Fig. 4 is less pronounced for smaller viscosities: the error produced by the blended algorithm is smaller than the one produced by the implicit procedure over a longer period. The blended algorithm will however be used for the following simulations after having adjusted the blending parameter to the model.

3. ADIMENSIONNAL PARAMETERS

The parameter $m^*\zeta$ (or multiples of it like the Scruton number or the Skop-Griffin number) is adapted to determine whether the cylinder response is composed of two or three branches, but for a given response shape, it remains to determine the best parameter which collapses the different response regimes of the cylinder for a large interval of structural parameters. The reduced velocity U^* has often been used to plot the results (see Fig. 1) but the width of the amplitude peak varies with the mass of the system. A "true" reduced velocity U^*/f^* used in [9] seems to collapse ideally the results over a wide range of cylinder mass. However the adimensional parameters used in different studies are quite diversified and it is difficult to compare the results between them. This comes from the different techniques employed to make the cylinder equation adimensional. The general equation of the oscillator with structural damping reads:

$$m\ddot{y}(t) + c\dot{y}(t) + ky(t) = F_y(t) \quad \textbf{(3)}$$

where m is the cylinder mass, c is the structural damping, k is the rigidity and F_y is the resultant of the lift force. The natural frequency f_o of the cylinder defined above (see Eq. [2]) and the frequency f_h in water (defined by Eq. [4]) are often used in the adimensionalisation process.

$$f_h = \frac{1}{2\pi}\sqrt{\frac{k}{m+m_a}} \text{ with } m_a \approx m_d = \rho\pi R^2 L \quad \textbf{(4)}$$

The frequency in water depends on the added mass m_a which can be approximated here by the displaced mass of water m_d since the cylinder is placed in an infinite domain and the viscosity is small. The sets of adimensional parameters listed in Tab. 3 will be adopted here to compare our results. D is the cylinder diameter and L its length. U_∞ is the inlet velocity and ρ is the density of the fluid.

Table 3. Adimensional sets of parameters commonly used

Adimensional parameter	[8]	[9]	[19]
Amplitude A^*	y/D	y/D	y/D
Frequency f^*	f/f_0	f/f_h	fD/U_∞
Velocity U^*	$U_\infty/(f_0 D)$	$U_\infty/(f_h D)$	$U_\infty/2\pi f_0 D$
Mass m^*	m/m_d	m/m_d	$m/(0.5\rho D^2 L)$
Damping ζ	$c/\sqrt{km}$	$c/\sqrt{k(m+m_d)}$	$c/(0.5\rho U_\infty D L)$

The frequency f is the actual frequency of the cylinder, i.e. its oscillation frequency in response of VIV. The variables used by Shiels et al. [19] have been especially developed to by-pass the problem of definition for the structural frequencies f_o and f_h in extreme cases where k and/or m are null. A complementary adimensional rigidity $k^* = k/(0.5\rho U_\infty^2 L)$ is also introduced in [19]. The natural frequency f_o is only found in the expression of the velocity, but this variable is only used to compare the results with others, when the structural frequency exists. A new parameter called the so-called *effective rigidity* is finally defined as:

$$k_{eff}^* = k^* - 4\pi^2 f^{*2} m^* \quad \textbf{(5)}$$

This parameter is always defined, even if the mass or the rigidity (or both) are null. Moreover, it collapses very well the data for different structural parameters.

4. RESPONSE OF THE CYLINDER UNDERGOING VORTEX INDUCED VIBRATIONS

The model used for the simulations is the same as the one used in the first part of the study [18]. However, the oscillations of the cylinder are not imposed anymore, but they are induced by the incident flow. A first series of simulations are performed without structural damping and thus the movement is governed by Eq. (1). The time integration is realized with the blended algorithm, but further simulations are currently tested with the implicit procedure. Our results are compared to those of Shiels et al. [19] and to those of Khalak & Williamson [9].

The behaviour of the cylinder is summarized on the curves plotted on Fig. 5. The response regimes for the amplitude, the actual frequency of the cylinder and the aerodynamic coefficients are plotted against k_{eff}^* (see Eq. [5]). The amplitude response is only composed of the lower branch because the Reynolds number is low [9]. The results show a very good agreement with those of Shiels et al., for each parameter. A "resonant" zone is observed in the range $[0-5]$, where the maximal amplitude of oscillation reaches $A^* = 0.58$ at $k_{eff}^* = 2.32$. The peak of amplitude is naturally associated with an increase of the aerodynamic coefficients. The values of the lift coefficient plotted are the maximal values, as the mean fluctuating lift is null. This is not true for the mean drag coefficient which is plotted on the last graph. A detailed analysis of three cases ($k_{eff}^* = 17.5$, $k_{eff}^* = 2.32$ and $k_{eff}^* = 0.05$) is done in the following paragraphs; the frequency content, vortex shedding modes and lock-in zone are studied and the phenomena observed are linked together.

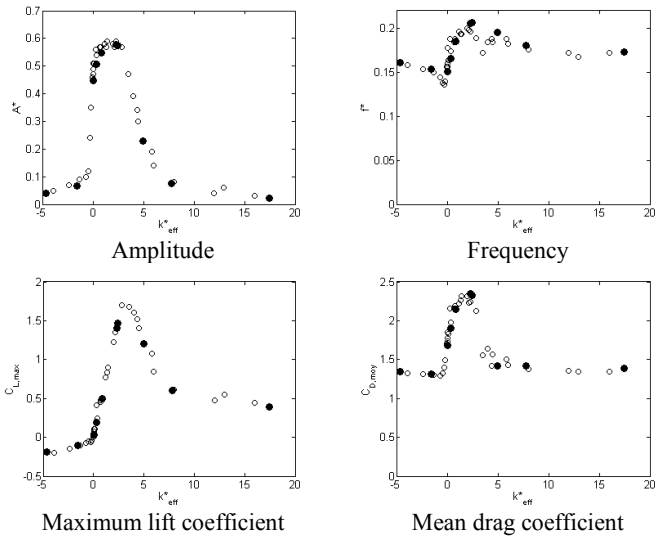

Figure 5. Amplitude, frequency and aerodynamic response of the cylinder undergoing VIV

4.1. Frequential content and phase portraits

Time histories of the cylinder displacement are now very interesting data, because the movement is not known a priori as it was the case for forced vibrations. The graphs in the left column (Fig. 6) show the difference of amplitude obtained between the different regimes. In the "resonant" zone, the amplitude is maximal but remains limited. This is due to the self-limitation phenomenon mentioned in the introduction. The periodic regime is reached quickly: about ten cycles only are necessary for the maximal amplitude response. The corresponding FFT of the cylinder displacement response are plotted versus the frequency ratio $f^* = f / f_h$. It can be seen that the peak moves from the left to the right as k_{eff}^* decreases. For $k_{eff}^* = 2.32$, $f^* = 1$ indicates that the cylinder oscillates at the natural frequency of the structure instead of the Strouhal frequency f_S for a Reynolds number $\mathrm{Re} = 100$. The Strouhal frequencies at $\mathrm{Re} = 100$ in the three cases are given in Tab. 4. The values corresponding to $k_{eff}^* = 0.05$ and $k_{eff}^* = 17.5$ indicate that in these two cases, the oscillations of the cylinder are driven by the Strouhal frequency, because the peak of the FFT is at $f^* = f_S / f_h$.

When k_{eff}^* is increased, the cylinder response exhibits an amplification of the amplitude and aerodynamic coefficients which can be related to the synchronization of the cylinder frequency on its natural frequency: this is typical for the lock-in zone, which has been defined as the domain where the cylinder frequency shifts from the Strouhal frequency and is locked on the structural one.

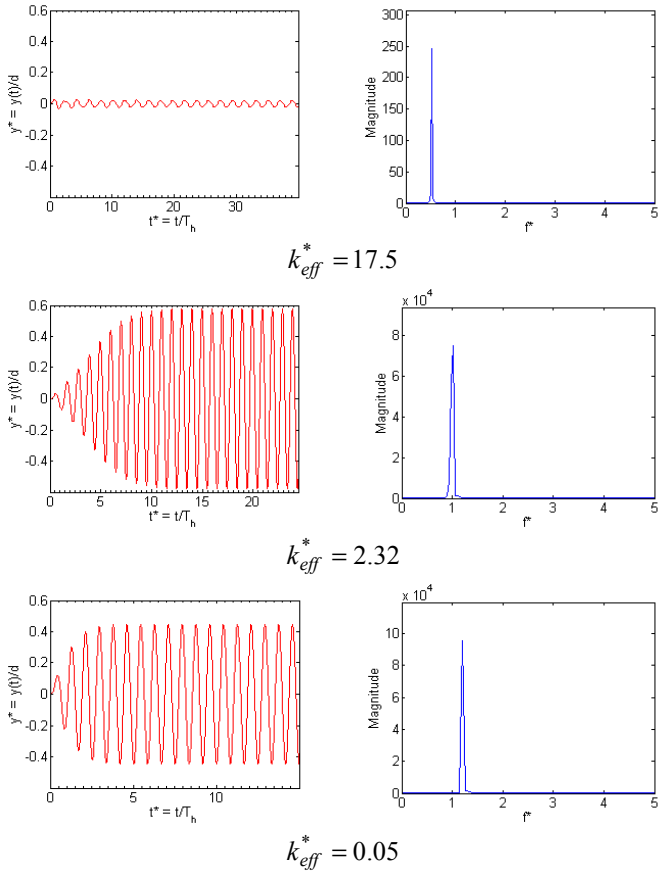

Figure 6. Time histories and FFT of the cylinder displacement

Table 4. Strouhal frequencies for a fixed cylinder

k_{eff}^*	0.05	2.32	17.5
f_S / f_h	1.35	0.82	0.51

The phase portraits of the oscillator are represented on Fig. 7. The amplification of the lift coefficient is still visible on the second portrait. The global inclination of the portrait is always in the first quadrant meaning that the phase angle between the lift force and the displacement remains in the interval $[0° - 45°]$: no phase jump is observed. For higher Reynolds numbers, a phase jump appears generally at about $U^* = 5.6$ [8], [9], i.e. when the amplitude increases sharply. One reason for the absence of phase jump can be the low Reynolds number used, which prohibits the modification of the vortex shedding mode as it will be seen later.

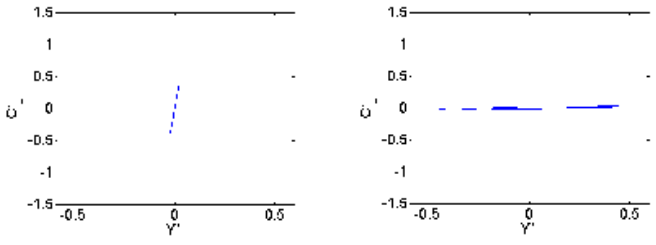

$k_{eff}^{*} = 17.5$ $k_{eff}^{*} = 0.05$

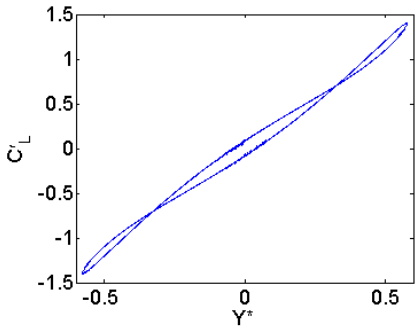

$k_{eff}^{*} = 2.32$

Figure 7. Phase portraits of the cylinder

The convergence towards the limit cycle has also been tested to check if the equilibrium state reached was stable or not. A new simulation is performed at $k_{eff}^{*} = 2.32$ with an initial velocity imposed equal to the incident flow speed. The "true" phase portraits (adimensional velocity against displacement) are plotted in the two cases on Fig. 8. The limit cycle is the same, which means that the state reached is stable, whatever the initial condition may be.

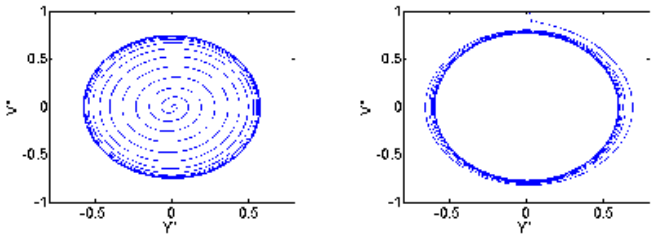

Figure 8. Convergence towards the limit cycle with null $(Y^{*},V^{*})=(0,0)$ or non null $(Y^{*},V^{*})=(0,1)$ initial condition

4.2. Vortex shedding modes

The vortex shedding patterns are illustrated on Fig. 9 with the vorticity field. The vortices are shed alternately from the upper and lower sides of the cylinder, according to the classical Von Karman streets or 2S mode. The shedding mode is very similar to the results of Shiels et al. [19], but no clear modification of the wake has been observed. The vortices are more stretched in the vertical direction at $k_{eff}^{*} = 2.32$ than in the other cases. This slight modification is certainly due to the increased amplitude of oscillation in the intermediate case, which deforms the wake in the vertical direction.

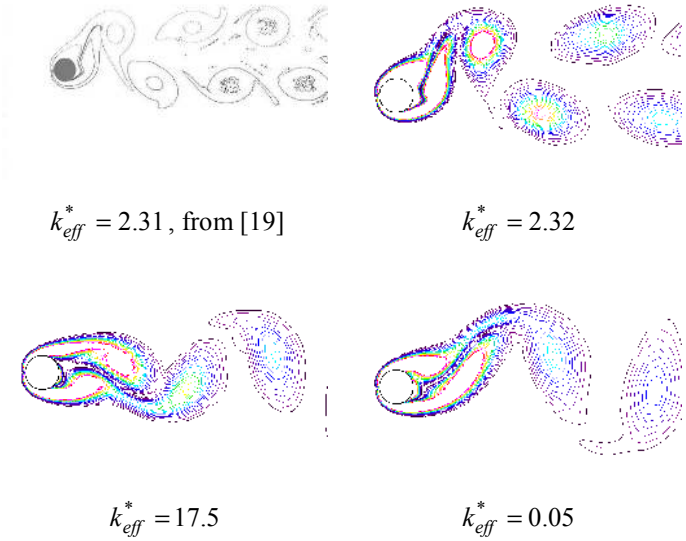

$k_{eff}^{*} = 2.31$, from [19] $k_{eff}^{*} = 2.32$

$k_{eff}^{*} = 17.5$ $k_{eff}^{*} = 0.05$

Figure 9. Vortex shedding modes inside and outside the lock-in zone

For higher Reynolds numbers, a change between a 2S and 2P mode is often observed (see [8], [9]) and can be linked to the transition between the upper and lower branch of excitation (see Fig. 1). This transition has also been connected to the phase jump in the case of forced oscillations or VIV. However, the low Reynolds number used here prohibits the change of the mode shape. Moreover, the numerical simulations fail sometimes to capture this mode change, even if the Reynolds number is high: in their study Al-Jamal & Dalton [2] do not obtain the 2S and 2P modes although they use Large Eddy Simulations at $\mathrm{Re} = 8000$. The authors argue that these modes are only observed for sinusoidal oscillations. When oscillations are not purely sinusoidal, as it is the case in VIV for certain reduced velocities, the 2S, 2P, etc… structures may not become fully established because the amplitude of oscillation and phase angle are both time dependent. The lack of constancy in amplitude and phase angle could likely lead to the lack of repeatability in vortex formation which certainly could suppress the standard mode patterns.

The oscillations of the cylinder are not always purely sinusoidal and a beating behaviour is observed for example at $k_{eff}^{*} = 7.79$ (i.e. $U^{*} = 4.00$) as it is illustrated on Fig. 10. The displacements are not periodic between two successive cycles, but over several cycles. The spectrum exhibits therefore two

peaks, between f^*=0.68 and 1. The first value corresponds to the Strouhal frequency whereas the second is the cylinder natural frequency. The beating behaviour can be understood as a desynchronization phenomenon: the cylinder oscillation frequency progressively shifts from the natural frequency f_h, which is predominant at $k^*_{eff} = 2.32$, to the Strouhal frequency which drives the wake at $k^*_{eff} = 17.5$. There is a progressive change of the main peak in the spectrum, which is the sign of the response modification.

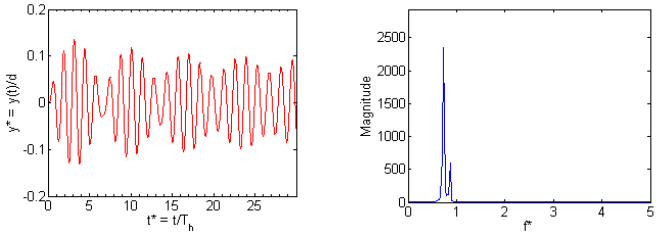

Figure 10. Beating behavior observed at k^*_{eff}=7.79

This beating behaviour is often observed [2], [9], [14], [19] and has been related to a mode change, or a *mode competition*. Khalak & Williamson [9] have shown that this beating is associated which the transition between the lower and upper branch of excitation, and therefore with the transition between the 2S and 2P modes. We do not have a significant mode change, but the beating is however connected to the little modification of the vortex patterns between $k^*_{eff} = 2.32$ and $k^*_{eff} = 17.5$. Finally, the low Reynolds number prohibits the observation of the classical mode change 2S to 2P, but a little modification of the wake appears and a similar beating phenomenon happens, which is related to this vortex pattern change and to the progressive transition between a cylinder response driven by the natural frequency f_o to a response driven by the Strouhal frequency f_S.

4.3. Lock-in zone

The amplitude response plotted on Fig. 5 has shown an amplification over a certain range of k^*_{eff} or reduced velocity U^* defined by Khalak & Williamson (see Tab. 3). This latter parameter is often used to plot the response, instead of k^*_{eff}. The "resonant" zone can also be easily identified by plotting the frequency response with the adimensional frequency $f^* = f / f_h$ used in [9]. The evolution is presented on Fig. 11. The horizontal line $f^* = 1$ indicates that the cylinder oscillation frequency is the natural frequency. On the contrary, the oblique lines give the Strouhal frequencies over the range of reduced velocities studied. Two lines are represented since the results of Khalak and Williamson are obtained at higher Reynolds numbers where the Strouhal number is slightly greater. From the results of [9], it can be seen that for small or high U^*, the cylinder oscillations are driven by the Strouhal. In the range $[4-6]$, the cylinder frequency f is exactly equal to the natural frequency of the cylinder: this is the upper branch. Over the range $[6-10]$, the frequency f is still not equal to the Strouhal frequency but to a multiple of the natural frequency f_h: this is the lower branch. The interval $[4-10]$ can be defined as the lock-in zone because the cylinder frequency shifts from the Strouhal frequency. The transition zone between the upper and lower branch is characterized by the simultaneous existence of two frequencies in the response.

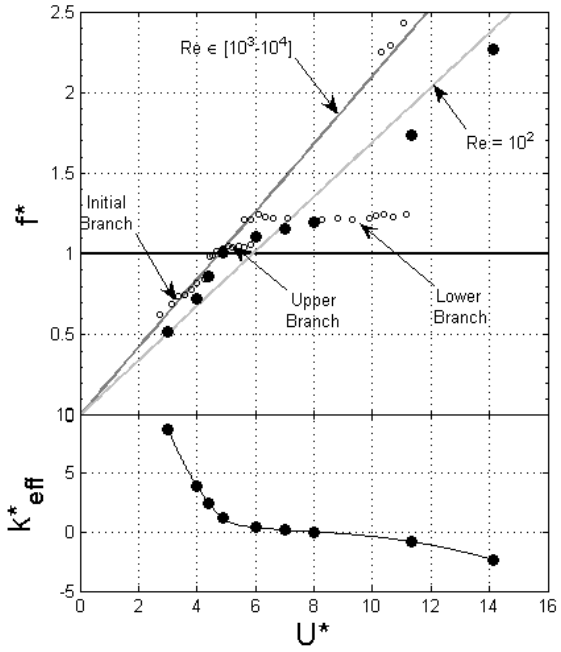

Figure 11. Frequency response and lock-in zone. ● Present simulation, ○ Khalak & Williamson [9]

In our case, the response is less complex since the upper and lower branches are not observed. However, the two first and last points ($U^* = 3-4$ and $U^* = 11.32-14.12$) show that the cylinder oscillations are in this case driven by the Strouhal frequency. In the range $[4.4-11.32]$, the actual frequency of the cylinder shifts from the Strouhal frequency and follows an oblique line whose slope is very smooth and quasi horizontal. Over this interval, the cylinder is locked on, near the natural frequency of the cylinder. In the present case, the lock-in zone is not exactly horizontal but rather oblique. This is due to the mass of the system as it is shown by Shiels et al. In [19], the authors perform several series of simulations for different mass ratios m^* between 0 and 20. For small masses, the

lock-in zone is not very pronounced. On the contrary, for high mass ratios the lock-in zone is immediately visible and forms a horizontal zone located at $f^* = 1$. In most cases tested here, we choose a mass ratio $m^* = 3.3$, which explains the absence of strictly horizontal level. There is no evident relation between the effective rigidity k_{eff}^* of Shiels et al. and the reduced velocity U^* used by Khalak & Williamson because k_{eff}^* is defined from the actual cylinder oscillation frequency f which is not known a priori. The relation between the two parameters is given in the subplot on Fig. 11 to facilitate the link with the previous paragraphs.

5. FURTHER DEVELOPMENTS

The results presented before have been obtained for a low Reynolds number without structural damping. These assumptions have been made to begin with relatively simple models. In the future, our aim is to work with structural damping in order to try to capture the lower and upper branches of excitation and at higher Reynolds numbers which would be nearer from industrial applications.

The structural damping can be easily introduced in the coupling procedure used to integrate the cylinder motion. The equation solved is now Eq. (3). The blended scheme is adapted by adding only a damping term in the expression of the acceleration (Step 2 of the algorithm):

$$a^{n+1} = \frac{F_y^n}{m} - \frac{k}{m}x^n - \frac{c}{m}\dot{x}^n \qquad (6)$$

For the implicit procedure, the modification is not more difficult. Indeed, the iterative scheme (extensively presented and studied in [21]) is not modified by the introduction of the damping: the evaluation of the velocity by the Newton-Raphson method is not affected since the gradient is obtained with the acceleration which has been computed before with (6). Comparisons between the explicit, blended and implicit schemes have been performed for the configuration exposed on Fig. 2. The difference is that there is now a combination between numerical, viscous and structural damping. The results are not presented here but it is worth mentioning that the implicit procedure remains the best. The blended algorithm still provides an accurate solution and is a straightforward procedure to study the coupled problem.

Another difficulty arises from the increase of the Reynolds number which is synonymous with the apparition of turbulence. The present study has been conducted for $\mathrm{Re} = 100$, i.e. a Reynolds number small enough to have a laminar wake. The Reynolds number is now multiplied by ten and solutions must be found to take into account the turbulence of the wake. The Navier-Stokes equations are thus averaged and the fluctuations introduced by the turbulence are modelled by the Reynolds tensor. This latter is evaluated with a turbulent viscosity which depends on the turbulent kinetic energy and the specific dissipation rate. These variables are obtained by solving transport equations which are deduced from the Navier-Stokes equations. Finally the flow is computed with the classical Navier-Stokes equations, completed by a turbulence model composed of two transport equations. Among the numerous models existing, we choose the k-ω SST model developed by Menter [13]. This model combines the classical $k-\omega$ and $k-\varepsilon$ turbulence models and is particularly adapted to capture the recirculation zones after airfoils or bluff bodies. It has been successfully used by Le Pape & Lecanu [12] for profiles in wind engineering or by Guilmineau & Queutey [8] in the case of a cylinder undergoing VIV like ours.

The model has been first tested for a fixed cylinder. The Strouhal frequency found $St = 0.23$ is slightly greater than the empirical value $St = 0.21$ given by Norberg [16] but is in good agreement with other numerical studies: $St = 0.25$ in [14], $St = 0.23$ in [2]. The error remains small but the evaluation of the fluctuating lift is more difficult. The rms value computed is very far from the one proposed by Norberg. Indeed, for $\mathrm{Re} = 1000$, the rms values exhibits a wide scattering (see [16] for more details) and it is difficult to find a good agreement. This could explain the results obtained for VIV simulations at $\mathrm{Re} = 1000$.

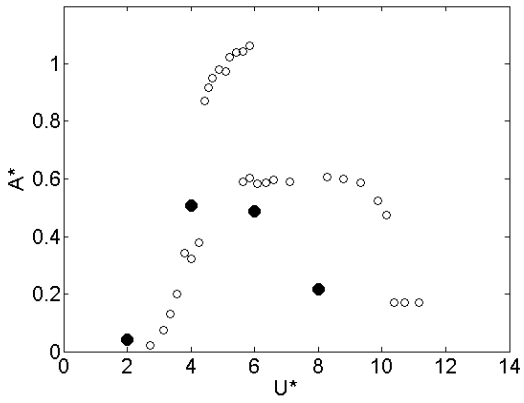

Figure 12. Amplitude response at Re=1000 and $m^*\zeta$=0.013.
● Present simulation, ○ Khalak & Williamson [9]

The simulations are performed with the $k-\omega$ SST turbulence model and the blended procedure to take into account the effect of the high Reynolds number and the coupling between the flow and the cylinder displacement respectively. Only four cases have been tested for reduced velocities ranging from $U^* = 2$ to $U^* = 10$. The graph on Fig. 12 shows the amplitude response of the cylinder at $\mathrm{Re} = 1000$ for a combined mass-damping parameter $m^*\zeta = 0.013$, a value equal to the one used in [8] and [9].

It can be seen that the amplitude is not always accurately evaluated. However the shape of the amplitude curve is respected, apart from the upper branch. For high reduced velocities, the amplitude is under-evaluated and falls rapidly. The upper branch does not seem to be reached, but more tests should be conducted in the range $U^* = 4 - 6$ to confirm this. Moreover, further developments are actually made to use the implicit procedure. This latter would perhaps provide a better description of the flow field and we hope that the upper branch could be reached, without using an increase or a decrease of the reduced velocity, as used in [8].

6. CONLUSION

The numerical results detailed in the present paper have proved that our industrial code is able to represent the vortex induced vibration phenomenon. Restrictions must be taken into account since the results are for instance in good agreement for low values of the Reynolds number and without structural damping. In this case, the response amplitude, frequency content and mode patterns correspond to others experimental or numerical studies. For higher Reynolds numbers the results are not yet very satisfactory: the amplitude response is under-evaluated for high reduced velocities. However further developments are actually made to understand the effects of the structural damping and the higher Reynolds number. This needs to analyze on the one hand the effect of the structural damping at low Reynolds numbers (i.e. without turbulence), and on the other hand the influence of the turbulence model by testing several ones. Interesting results could then be obtained by using the implicit procedure which would certainly provide a better description of the flow field.

REFERENCES

[1] D. ABOURI. *Un algorithme d'interaction fluide-solide rigide : application à la volumétrie*. PhD Thesis, Université de Poitiers, 2003.

[2] H. AL-JAMAL, C. DALTON. Vortex Induced Vibrations Using Large Eddy Simulation at a Moderate Reynolds Number. *Journal of Fluids and Structures*, **19**, 73-92, 2004.

[3] P. ANAGNOSTOPOULOS, P.W. BEARMAN. Response Characteristics of a Vortex-Excited Cylinder at Low Reynolds Numbers. *Journal of Fluids and Structures*, **6**, 39-50, 1992.

[4] C. FARHAT, M. LESOINNE, P. STERN. High Performance Solution of Three-Dimensional Nonlinear Aeroelastic Problems via Parallel Partitioned Algorithms: Methodology and Preliminary Results. *Advances in Engineering Software*, **28**, 43-61, 1997.

[5] J.H. FERZIGER, M. PERIC. *Computational Methods for Fluid Dynamics*. Springer-Verlag, 1996.

[6] R.J. FRITZ. The Effects of Liquids on the Dynamic Motions of Immersed Solids. *Journal of Engineering for Industry*, 167-173, 1972.

[7] M. GLÜCK, M. BREUER, F. DURST, A. HALFMANN, E. RANK. Computation of Wind-Induced Vibrations of Flexible Shells and Membranous Structures; *Journal of Fluid and Structures*, **17**, 739-765, 2003.

[8] E. GUILMINEAU, P. QUEUTEY. Numerical Simulation of Vortex-Induced Vibration of a Circular Cylinder with Low Mass-Damping in a Turbulent Flow. *Journal of Fluid and Structures*, **19**, 449-466, 2004.

[9] A. KHALAK., C.H.K. WILLIAMSON. Motions, Forces and Mode Transitions in Vortex-Induced Vibrations at Low Mass-Damping, *Journal of Fluids and Structures*, **13**, 813-851, 1999.

[10] B. KOOBUS, C. FARHAT. Second Order Time-Accurate and Geometrically Conservative Implicit Schemes for Flow Computations on Unstructured Dynamic Meshes, *Computer Methods in Applied Mechanics and Engineering*, **170**, 103-129, 1999.

[11] C. LEBLOND, A. PLACZEK, J.F. SIGRIST. *Analytical and Numerical Calculation of Added Mass and Added Damping for a Rigid Cylinder in Cylindrical Fluid Confinement*. Pressure Vessel and Piping, San Antonio, 22-26 July 2007.

[12] A. LE PAPE, J. LECANU. 3D Navier-Stokes Computations of a Stall-Regulated Wind Turbine. *Wind Energy*, **7**, 309-324, 2004.

[13] F.R. MENTER. Two-Equation Eddy-Viscosity Turbulence Models for Engineering Applications. *AIAA Journal*, **32**, 598-605, 1994.

[14] S. MITTAL, V. KUMAR. Flow-Induced Vibrations of a Light Circular Cylinder at Reynolds numbers 10^3 to 10^4. *Journal of Sound and Vibration*, **245** (5), 923-946, 2001.

[15] D. NEWMAN, G.E. KARNIADAKIS. Simulation of Flow Over a Flexible Cable: a Comparison of Forced and Flow-Induced Vibration. *Journal of Fluid and Structures*, **10**, 439-453, 1996.

[16] C. NORBERG. Fluctuating Lift on a Circular Cylinder : Review and New Measurements. *Journal of Fluids and Structures*, **17**, 57-96, 2003.

[17] S. PIPERNO. *Simulation numérique de phénomènes d'interaction fluide-structure*. PhD Thesis, Ecole Nationale des Ponts et Chaussées, 1995.

[18] A PLACZEK, J.F. SIGRIST, A. HAMDOUNI. *Numerical Simulation of Vortex Shedding Past a Circular Cylinder in a Cross-Flow at Low Reynolds Number with Finite-Volume Technique. Part 1: Forced Oscillations*. Pressure Vessel and Piping, San Antonio, 22-26 July 2007.

[19] D. SHIELS, A. LEONARD, A. ROSHKO. Flow-Induced Vibration of a Circular Cylinder at Limiting Structural Parameters. *Journal of Fluid & Structures*, **15**, 3-21, 2001.

[20] J.F. SIGRIST. *Modélisation et simulation numérique d'un problème couplé fluide/structure non-linéaire. Application au dimensionnement de structures nucléaires de propulsion navale*. PhD Thesis, Université de Nantes, 2004.

[21] J.F. SIGRIST, D. ABOURI. *Numerical Simulation of a Non-Linear Coupled Fluid-Structure Problem With Implicit and Explicit Coupling Procedures*. Pressure Vessel and Piping, Vancouver, 22-28 July 2006.

[22] A.K. SLONE, K. PERICLEOUS, C. BAILEY, M. CROSS. Dynamic Fluid-Structure Interaction Using Finite-Volume Unstructured Mesh Procedures. *Computers & Structures*, **80**, 371-390, 2002.

View publication stats